JOURNAL OF GUIDANCE, CONTROL, AND DYNAMICS
Vol. 29, No. 2, March–April 2006

Evolutionary Search for Deep-Space Science Mission Orbits

Pini Gurfil*
Technion—Israel Institute of Technology, 32000 Haifa, Israel
and
N. Jeremy Kasdin†
Princeton University, Princeton, New Jersey 08544

We present an application of an evolutionary programming method, niching genetic algorithms, to the search for orbits in the spatial elliptic restricted three-body problem (ER3BP) that is suitable for deep-space science missions. The niching method used is deterministic crowding, which renders a global optimization while permitting for several optimal and suboptimal solutions to coexist. This novel approach yields diverse probing of the state space of the ER3BP. From the practical standpoint, the orbits found remain within a bounded distance from Earth, thus allowing high data-rate communication while ensuring safe operational environment, far from thermal perturbations and visual occultation as well as Earth's magnetic and radiation fields.

Nomenclature

a	=	semimajor axis
d	=	distance function
E	=	eccentric anomaly
e	=	eccentricity
f	=	fitness function
$\boldsymbol{f}$	=	vector-valued function
$\boldsymbol{R}$	=	position vector relative to sun
$\boldsymbol{r}$	=	position vector relative to Earth
$\boldsymbol{x}$	=	state vector
θ	=	true anomaly
μ	=	normalized gravitational parameter
μ_E	=	gravitational constant of the Earth
μ_S	=	gravitational constant of the sun
ω	=	orbital angular velocity
$\| \|$	=	Euclidean vector norm

Subscript

0	=	initial value

Superscripts

$*$	=	dimensional quantity
$\hat{}$	=	normalized quantity
$'$	=	differentiation with respect to true anomaly
$\cdot$	=	time differentiation

I. Introduction

OVER the next few decades, NASA and ESA have planned a variety of deep-space science missions such as ESA's Darwin and NASA's Terrestrial Planet Finder (TPF).[‡,§] These missions pose many orbit design challenges. Astrophysical observatories must be separated from Earth by a large distance to minimize stellar occultation, thermal perturbations, and environmental effects such as the magnetic and radiation fields. The spacecraft must also remain within a specified distance to maintain high data rate communication. It is also desirable to eliminate or minimize stationkeeping.

To satisfy the constraints, several viable trajectories have been proposed. For example, the James Webb Space Telescope mission has considered[¶] a halo orbit around the sun–Earth collinear Lagrangian libration point L_2. For the TPF mission L_2, Earth-trailing and Earth drift-away orbits have been examined.[1] Other missions have planned arrested drift-away trajectories in which a single impulsive velocity change is used to keep the spacecraft within a rough formation relative to Earth.

The framework often adopted for preliminary orbit analysis and design is that of the planar or spatial circular restricted three-body problem (CR3BP) with the sun as the large primary and the Earth as the small primary. Investigation of the motion near the CR3BP collinear Lagrangian equilibrium points has yielded many families of trajectories. Lyapunov orbits obtained in the planar case[2] bifurcate into the northern and southern family of halo orbits.[3] Families of Lissajous orbits were also detected.[4]

Although the use of the CR3BP model has proven fruitful, this approach constitutes an approximation because Earth's orbital eccentricity about the sun is neglected. When the eccentricity is taken into account, the CR3BP becomes the elliptic restricted three-body problem (ER3BP). The incorporation of the eccentricity renders the analysis more involved. For example, in the ER3BP the location of the collinear libration points is pulsating with respect to Earth, and there is no closed-form solution for the nonautonomous integral of motion.

A wealth of literature exists on the ER3BP. Numerous works have considered derivation of periodic orbits in the planar case,[5–8] periodic orbits in the spatial case with a critical mass ratio of half[9] or a critical unit eccentricity,[10] approximate integrals of motion,[11,12] specialized regularization,[13] and the dynamics of libration points.[14] However, there has not been a derivation of orbits in the sun–Earth ER3BP based on a practical set of mission constraints.

This work is aimed at filling this gap by performing a systematic characterization of families of candidate orbits and comparing the results to known solutions for orbits about the small primary, as obtained by Hénon.[15] Hénon restricted his search to two-dimensional, simple-periodic symmetrical orbits. We do not restrict the work to finding planar periodic orbits, but rather we explore orbits that do not violate the prespecified mission constraints, such as minimum and maximum distance from Earth and numerical stability (i.e., orbits

Presented as Paper 2002-4539 at the AIAA/AAS Astrodynamics Specialist Conference, Monterey, CA, 5–8 August 2002; received 20 October 2004; revision received 6 February 2005; accepted for publication 10 February 2005.

*Senior Lecturer, Faculty of Aerospace Engineering; pgurfil@technion.ac.il. Senior Member AIAA.

†Assistant Professor, Mechanical and Aerospace Engineering Department; jkasdin@princeton.edu. Senior Member AIAA.

‡Data available online at http://sci.esa.int/home/darwin/index.cfm.

§Data available online at http://origins.jpl.nasa.gov.

¶Data available online at http://icarus.stsci.edu/~lubow/ngst/orbits.html.

do not diverge over relatively long timescales). Thus, we find new sets of three-dimensional orbits that were not found by Hénon.

We have chosen the ER3BP formulation from two main reasons. First, from the theoretical standpoint we are interested in showing existence of periodic orbits about Earth in the ER3BP (in spite of the fact that Earth's eccentricity is small and periodic solutions can be found by continuation from the CR3BP); and, from the practical standpoint, this model is computationally inexpensive, thus constituting a stepping stone for applying our methods to a full-ephemerides simulation, as elaborated upon in Sec. IV.B.

Characterization of the orbits is carried out using a novel approach. We perform a stochastic yet structured constrained search of initial conditions that maximize a given objective function. The stochastic search is performed using genetic algorithms (GAs), which are an optimization technique based on the Darwinian theory of the survival of the fittest.[16] GAs have been generating an increasing interest in the space community because of their potential applications in this field. Reference 17 suggests an optimal control design using GAs, Refs. 18 and 19 proposes a methodology for the design of optimal-transfer trajectories using GAs, and Ref. 20 uses GAs for detecting high-inclination orbits in the restricted three-body problem.

The GA optimization is performed for various lower and upper bounds on the initial conditions. This enables the characterization of many families of orbits. Each family contains topologically distinct orbits, which offer promising features for deep-space missions. The different families are then categorized according to various criteria to yield two- and three-dimensional distant retrograde orbits, distant prograde orbits, and highly elliptic orbits.

II. Equations of Motion

In most past research, a barycentric rotating-pulsating coordinate system has been used to model the ER3BP.[2] In this study, however, we have adopted Hill's rotating-pulsating coordinate system, which is particularly useful for characterization of distant orbits about the small primary (including motion with 1:1 commensurability). The origin of this coordinate system, denoted by $\hat{x}, \hat{y}, \hat{z}$, is at the center of Earth, as depicted in Fig. 1. The $\hat{x}$ axis is directed radially outward along the local vertical, the $\hat{y}$ axis lies along the direction of Earth motion, and the $\hat{z}$ axis is normal to the ecliptic to complete the Cartesian dextral setup.

Following the usual analysis, let $\boldsymbol{r} \in \mathbb{R}^3 \backslash \{\mathbf{0}\}$ denote the position vector of the vehicle relative to Earth, and $\boldsymbol{R} \in \mathbb{R}^3 \backslash \{\mathbf{0}\}$ that of the Earth relative to the sun. The acceleration of the spacecraft relative to Earth $\ddot{\boldsymbol{r}}$, evaluated in the coordinate system $\hat{x}, \hat{y}, \hat{z}$ assuming a control- and perturbation-free motion, can be written as

$$\ddot{\boldsymbol{r}} = -\frac{\mu_E \boldsymbol{r}}{\|\boldsymbol{r}\|^3} - \left[\frac{\mu_S(\boldsymbol{R}+\boldsymbol{r})}{\|\boldsymbol{R}+\boldsymbol{r}\|^3} - \frac{\mu_S \boldsymbol{R}}{\|\boldsymbol{R}\|^3}\right] \tag{1}$$

To facilitate the mathematical formulation, we use the following relationships and unit conventions. First, the sun–Earth relative position vector, expressed in the Earth-centered rotating frame, is $\boldsymbol{R} = [R, 0, 0]^T$. R is given by the usual two-body formulation describing the Earth's motion about the sun,

$$R = \frac{a(1-e^2)}{1+e\cos\theta} \tag{2}$$

where $e = 0.0167$ is the eccentricity. The semimajor axis is measured in astronomical units (AU), so that $a = 1\ \text{AU} = 1.496 \times 10^8$ km. The dimensional position vector, $\boldsymbol{r} = [\xi, \eta, \zeta]^T = [R \cdot x, R \cdot y, R \cdot z]^T$, is normalized by R, so that the normalized position vector becomes $\hat{\boldsymbol{r}} = [x, y, z]^T$. The independent variable is the true anomaly, where the relationship between the dimensional time and true anomaly is given by:

$$t^* = \sqrt{\left(a^3/\mu_S\right)}(E - e\sin E) \tag{3}$$

In Eq. (3), E is the eccentric anomaly, given by[2]

$$E = 2\tan^{-1}\left\{\sqrt{[(1-e)/(1+e)]}\tan(\theta/2)\right\} \tag{4}$$

Time is then normalized by the Earth mean heliocentric angular velocity, that is, $t = t^*/\sqrt{(a^3/\mu_S)}$. To normalize the velocity components, we note that

$$\frac{\mathrm{d}}{\mathrm{d}t^*} = \frac{\mathrm{d}\theta}{\mathrm{d}t^*}\frac{\mathrm{d}}{\mathrm{d}\theta} \tag{5}$$

where

$$\omega = \frac{\mathrm{d}\theta}{\mathrm{d}t^*} = \sqrt{\frac{\mu_E+\mu_S}{a^3(1-e^2)^3}}(1+e\cos\theta)^2 \tag{6}$$

Thus, the dimensional velocity vector, $\boldsymbol{v} = [\dot{\xi}, \dot{\eta}, \dot{\zeta}]^T = \omega[(R \cdot x)', (R \cdot y)', (R \cdot z)']^T$, can be normalized by $R\omega$, to yield the normalized velocity $\hat{\boldsymbol{v}} = [x', y', z']^T$. The acceleration is normalized by $R\omega^2$. Also, the normalized gravitation parameter is defined as usual by $\mu \triangleq \mu_E/(\mu_E+\mu_S) = 3.0034495182 \times 10^{-6}$.

To get the normalized equation of motion, we start from Eq. (1) and evaluate the expression for the inertial acceleration in the Earth-fixed rotating frame. The dimensional component-wise equations are

$$\ddot{\xi} - 2\omega\dot{\eta} - \ddot{\omega}\eta - \omega^2\xi = -\frac{\mu_E\xi}{(\xi^2+\eta^2+\zeta^2)^{\frac{3}{2}}} - \frac{\mu_S(\xi+R)}{[(\xi+R)^2+\eta^2+\zeta^2]^{\frac{3}{2}}} + \frac{\mu_S}{R^2} \tag{7a}$$

$$\ddot{\eta} + 2\omega\dot{\xi} + \dot{\omega}\xi - \omega^2\eta = -\frac{\mu_E\eta}{(\xi^2+\eta^2+\zeta^2)^{\frac{3}{2}}} - \frac{\mu_S\eta}{[(\xi+R)^2+\eta^2+\zeta^2]^{\frac{3}{2}}} \tag{7b}$$

$$\ddot{\zeta} = -\frac{\mu_E\zeta}{(\xi^2+\eta^2+\zeta^2)^{\frac{3}{2}}} - \frac{\mu_S\zeta}{[(\xi+R)^2+\eta^2+\zeta^2]^{\frac{3}{2}}} \tag{7c}$$

where R and ω are given by Eqs. (2) and (6), respectively.

Let

$$\boldsymbol{r} = [\xi, \eta, \zeta]^T = [Rx, Ry, Rz]^T \tag{8}$$

so that

$$\dot{\xi} = \dot{R}x + \dot{x}R, \qquad \dot{\eta} = \dot{R}y + \dot{y}R, \qquad \dot{\zeta} = \dot{R}z + \dot{z}R \tag{9}$$

Taking the derivatives gives

$$\ddot{\xi} = \ddot{R}x + \ddot{x}R + 2\dot{R}\dot{x}, \qquad \ddot{\eta} = \ddot{R}y + \ddot{y}R + 2\dot{R}\dot{y}$$
$$\ddot{\xi} = \ddot{R}z + \ddot{z}R + 2\dot{R}\dot{z} \tag{10}$$

Recall also that

$$\dot{R} = -R\dot{\omega}/2\omega, \qquad \ddot{R} = \omega^2[R - R^2/a(1-e^2)] \tag{11}$$

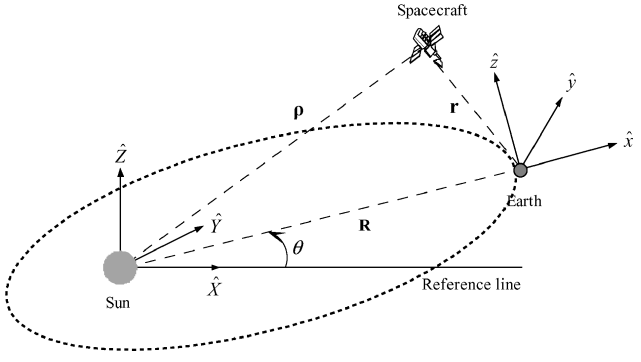

Fig. 1 Definition of coordinate systems.

Next, we substitute Eqs. (8–11) into Eqs. (7) and divide by $R\omega^2$. After canceling terms, we get

$$-\frac{R}{a(1-e^2)}x+\frac{\ddot{x}}{\omega^2}-\frac{\dot{\omega}\dot{x}}{\omega^3}-\frac{2\dot{y}}{\omega}=-\frac{\mu_E x}{R^3\omega^2(x^2+y^2+z^2)^{\frac{3}{2}}}$$
$$-\frac{\mu_S(x+1)}{R^3\omega^2[(x+1)^2+y^2+z^2]^{\frac{3}{2}}}+\frac{\mu_S}{R^3\omega^2} \tag{12}$$

$$-\frac{R}{a(1-e^2)}y+\frac{\ddot{y}}{\omega^2}-\frac{\dot{\omega}\dot{y}}{\omega^3}-\frac{2\dot{x}}{\omega}=-\frac{\mu_E y}{R^3\omega^2(x^2+y^2+z^2)^{\frac{3}{2}}}$$
$$-\frac{\mu_S y}{R^3\omega^2[(x+1)^2+y^2+z^2]^{\frac{3}{2}}} \tag{13}$$

$$\left[1-\frac{R}{a(1-e^2)}\right]z+\frac{\ddot{z}}{\omega^2}-\frac{\dot{\omega}\dot{z}}{\omega^3}=-\frac{\mu_E z}{R^3\omega^2(x^2+y^2+z^2)^{\frac{3}{2}}}$$
$$-\frac{\mu_S z}{R^3\omega^2[(x+1)^2+y^2+z^2]^{\frac{3}{2}}} \tag{14}$$

Using Eq. (5), we observe that

$$\dot{x}=\omega x', \qquad \ddot{x}=\omega\omega' x' \tag{15}$$

and similarly for y and z.

Substituting Eqs. (15) into the left side of Eqs. (7), using Eq. (2), and noticing that

$$\frac{\mu_S}{R^3\omega^2}=(1+e\cos\theta)^{-1}(1-\mu), \qquad \frac{\mu_E}{R^3\omega^2}=(1+e\cos\theta)^{-1}\mu \tag{16}$$

yields the desired normalized equations of motion in the Earth-centered rotating-pulsating reference frame:

$$x''=2y'+(1+e\cos\theta)^{-1}\times\left\{x-\frac{\mu x}{(x^2+y^2+z^2)^{\frac{3}{2}}}-\frac{(1-\mu)(x+1)}{[(x+1)^2+y^2+z^2]^{\frac{3}{2}}}+1-\mu\right\} \tag{17}$$

$$y''=-2x'+(1+e\cos\theta)^{-1}\times\left\{y-\frac{\mu y}{(x^2+y^2+z^2)^{\frac{3}{2}}}-\frac{(1-\mu)y}{[(x+1)^2+y^2+z^2]^{\frac{3}{2}}}\right\} \tag{18}$$

$$z''=-z+(1+e\cos\theta)^{-1}\times\left\{z-\frac{\mu z}{(x^2+y^2+z^2)^{\frac{3}{2}}}-\frac{(1-\mu)z}{[(x+1)^2+y^2+z^2]^{\frac{3}{2}}}\right\} \tag{19}$$

The state-space representation of Eqs. (17–19) can be written as

$$\boldsymbol{x}'=\boldsymbol{f}(\boldsymbol{x},\theta) \tag{20}$$

where

$$\boldsymbol{f}:\mathbb{R}^3\backslash\{0\}\times\mathbb{R}^3\times\mathbb{S}^1\to\mathbb{R}^6$$
$$\boldsymbol{x}\triangleq[\hat{\boldsymbol{r}}\quad\hat{\boldsymbol{v}}]^T=[x,y,z,x',y',z']^T\in\mathbb{R}^3\backslash\{0\}\times\mathbb{R}^3 \tag{21}$$

The inertial reference frame used here is a heliocentric-ecliptic coordinate system, denoted by $\hat{X}$, $\hat{Y}$, $\hat{Z}$, as shown in Fig. 1. By using the preceding unit convention, the transformation of some position vector $\boldsymbol{p}$ from the rotating frame to the inertial frame is given by

$$[\boldsymbol{p}]_{\hat{X},\hat{Y},\hat{Z}}=\begin{bmatrix}\cos\theta & -\sin\theta & 0\\ \sin\theta & \cos\theta & 0\\ 0 & 0 & 1\end{bmatrix}\left\{[\boldsymbol{p}]_{\hat{x},\hat{y},\hat{z}}+\begin{bmatrix}R\\0\\0\end{bmatrix}\right\} \tag{22}$$

III. Optimal Orbit Characterization

The use of traditional optimization methods (such as the gradient search and the simplex method) to search for initial conditions yielding orbits with prespecified properties can fail because of the rich dynamical structure and sensitive dynamics of the ER3BP. Thus, the search needs to be global, that is, performed over some given range of permissible initial conditions. (The optimization space in our search problem is spanned by the distribution of initial conditions.) GAs offer a convenient solution to this problem.

A. Genetic Algorithms

Genetic algorithms possess a number of specialized features compared to traditional optimization procedures: First, they work with a coding (usually binary) of the parameter set ("strings," in the GA terminology) instead of the parameters themselves. Second, they search from a population of initial conditions instead of a single point. Third, they use only objective function ("fitness") evaluations instead of derivatives or other auxiliary information. Fourth, they use probabilistic transition rules instead of deterministic rules.

The GA most commonly used in engineering applications is the so-called simple GA. To perform the evolutionary search, the simple GA uses the operators of crossover, reproduction, and mutation. Crossover is used to create new solution strings ("children" or "offspring") from existing strings ("parents"). Reproduction copies individual strings according to the objective function values. Mutation is an occasional random alteration of the value of a string position, used to promote diversity of solutions.

Although simple GAs are capable of detecting the global optimum,[16] they suffer from two main drawbacks: first, convergence to a local optimum is possible by the effect of premature convergence, in which all individuals in a population become nearly identical before the optima has been located. Second, convergence to a single optimum does not reveal other optima, which can exhibit attractive features. To overcome these problems, modifications of simple GAs were considered. These modifications are called niching methods and are aimed at promoting a diversity of solutions for multimodal optimization problems. In other words, instead of converging to a single (possibly local) optimum, niching allows for a number of optimal solutions to coexist and lets the designer choose the appropriate one. The niching method used throughout this study is deterministic crowding.[19,21] According to this method, individuals are first randomly grouped into parent pairs. Each pair generates two children by application of the standard genetic operators. Every child then competes against one of his parents. The winner of the competition moves on to the next generation. By denoting P_i for parent, C_i for child, $f()$ for fitness and $d()$ for distance, the pseudocode for the two possible parent–child tournaments can be written as

If $[d(P_1,C_1)+d(P_2,C_2)=d(P_1,C_2)+d(P_2,C_1)]$

If	$f(C_1)\geq f(P_1)$	replace	P_1	with	C_1
If	$f(C_2)\geq f(P_2)$	replace	P_2	with	C_2

Else

If	$f(C_1)\geq f(P_2)$	replace	P_2	with	C_1
If	$f(C_2)\geq f(P_1)$	replace	P_1	with	C_2

In addition to applying the deterministic crowding niching method, we have also used two-point crossover instead of a single-point crossover. In simple GA, the crossover operator breaks the binary string of parameters, the "chromosome," in a random point and exchanges the two pieces to create a new chromosome. In a two-point crossover, the chromosome is represented as a ring. The string between the two-crossover points is then exchanged. Two-point crossover or other multiple-point crossover schemes have preferable properties when optimizing highly nonlinear functions.[22]

B. Definition of the Objective Function, Constraints and Parameters

The constrained dynamic optimization problem of finding orbits about the small primary in the ER3BP can be formulated in a variety of ways. The resulting orbits depend on three main factors: the definition of the objective function, the search bounds on the initial conditions, and the minimum Earth-approach constraints. Different families of periodic and quasi-periodic orbits can be found for different formulations of the optimization problem. This notion is used to characterize the optimal orbits. For a given objective function, the lower and upper search bounds on initial conditions are changed in each optimization set, so that a diverse exploration (i.e., over various domains of the state space) of feasible orbits is obtained.

A few candidate formulations of the objective function were examined. The value of the initial true anomaly θ_0 was set to either 0 or π. Using θ_0 as an additional optimization parameter did not seem to be beneficial to the characterization process, as it simply yielded an orbital phase shift. After considering various objective function formulations, we found that the formulation which yielded the most significant results is as follows: find the optimal set of initial conditions $\boldsymbol{x}_0^*$ satisfying

$$\boldsymbol{x}_0^* = \arg\max_{x_0 \in X} \left\{ 1 \Big/ \left[r_{\max} - r_{\min})^2 + 1 \right] \right\} \tag{23}$$

where $r_{\min} \triangleq \min_{\theta \in [\theta_0, \theta_f]} \|\boldsymbol{r}\|$, $r_{\max} \triangleq \max_{\theta \in [\theta_0, \theta_f]} \|\boldsymbol{r}\|$, and X denotes a hyperrectangular domain defined by the upper and lower bound on initial conditions:

$$X \triangleq \{\boldsymbol{x}_0 : (\boldsymbol{x}_0)_{\min} \leq \boldsymbol{x}_0 \leq (\boldsymbol{x}_0)_{\max}\} \tag{24}$$

The objective function (23) was maximized subject to Eq. (24), the dynamic constraints of the equations of motion, and the inequality constraint

$$r_{\min} > R_E \tag{25}$$

where R_E is the (maximum) radius of Earth. The constraint (25) was used to rule out collision trajectories with Earth; it permits close Earth approaches, thus enabling us to identify orbits that can be used in future works as transfer trajectories to distant orbits (transfer orbits are outside the scope of the current text). Alternative constraints, such as limiting $r_{\min}$ to be larger than the moon's orbit semimajor axis, are possible, but will generally yield a more confined set of results.

Note that the objective function (23) is normalized to attain values between 0 and 1. This normalization facilitates the optimization procedure by regularizing the numerical values and preventing fitness function values to approach infinity as $r_{\min} \to r_{\max}$. The inverse-quadratic nature of the objective function facilitates the convergence of the optimization.

Table 1 Constants used in the GA optimization

Constant	Value
Mission lifetime	1 year
Population size	200
Number of generations	400
String length	32
Probability of crossover	0.999
Probability of mutation	0.001

Throughout the optimization, we have used the GA constants given in Table 1, where values for the probability of crossover, the probability of mutation, the number of generations, and the population size are listed. The mission lifetime selected was one year for all of the optimization sets. Although a typical mission lifetime can be longer, the one-year integration time considerably reduces the computer time required to perform the various optimization sets. After obtaining the optimal initial conditions, the integration is extended to five years. The integration is performed using a fourth-order Runge–Kutta integrator with relative and absolute tolerances of 10^{-10}. Each optimization batch takes about 6 h on a 2-GHz Pentium machine.

The values of $(\boldsymbol{x}_0)_{\min}$ and $(\boldsymbol{x}_0)_{\max}$ were selected to locate orbits outside Earth's sphere of influence. Combinations of $(\boldsymbol{x}_0)_{\min}$ and $(\boldsymbol{x}_0)_{\max}$ were selected such that the initial distance from Earth was larger than 1 million km (0.00668 AU) and smaller than 10 million km (0.0668 AU). The specific selection of the lower-bound value serves a two-fold purpose: first, it maximizes the number of orbits that lie away from Earth's perturbations; and second, it minimizes the number of Keplerian orbits, which in our case, are trivial two-body solutions. The different combinations of velocity component values were chosen such that the magnitude of the initial velocity would not exceed 15 km/s (0.5 AU/rad). The search space was limited in order to facilitate the numerical search (a smaller population size can be chosen for a smaller search space) and to avoid impractical orbits (either Earth drift-away, heliocentric orbits, or orbits that escape the sun–Earth system). Table 2 describes the actual upper and lower bounds used in each optimization set, as well as the true anomaly used for each set.

The specific selection of lower and upper bounds just mentioned loosely defines the actual maximum and minimum distance from Earth for each orbit. Nevertheless, to create a diverse and comprehensive characterization, we did not use hard constraints on the minimum and maximum distances of the vehicle from Earth. We emphasize that the purpose of the search is not confined to detecting orbits of particular shape or commensurability characteristics. We are seeking any orbit that can be suitable for a deep-space science mission according to the aforementioned constraints.

IV. Orbit Characterization Results

The eight GA optimization sets yielded many families of orbits. Some of the two-dimensional families (except family e, which we introduce shortly) are topologically equivalent to orbit families previously reported in the seminal work of Hénon.[15] However, Hénon's work analyzed Hill's problem, a special case of the general ER3BP setup. Moreover, the three-dimensional orbits are believed to constitute an important extension to Hénon's findings, as he searched for planar orbits only. We emphasize that the GA optimization searches over the state space of the full, three-dimensional, ER3BP.

A. Orbit Families

Because of the use of a niching GA, each optimization set can yield a few distinct solutions, which represent the global, and possibly a number of local, optima of the objective function within the search bounds. In this context, "family" is used to distinguish solutions that are known to be topologically different from one another, representing, roughly speaking, different values of the Jacobi integral (which is not constant in the ER3BP). Within a certain family,

Table 2 Description of the GA optimization sets

Optimization set no.	$(\boldsymbol{x}_0)_{\min}$	$(\boldsymbol{x}_0)_{\max}$	θ_0, rad	Resulting families
1	$[0.0066845, 0, 0, -0.5, 0, 0]^T$	$[0.066845, 0, 0, 0, 0, 0]^T$	0	f
2	$[0.0066845, 0, 0, 0, 0, 0]^T$	$[0.066845, 0, 0, 0.5, 0, 0]^T$	0	g'
3	$[0.0066845, 0, 0, 0, 0, 0]^T$	$[0.066845, 0, 0, 0.5, 0, 0]^T$	π	g'
4	$[0.0066845, 0, 0, -0.5, 0, 0]^T$	$[0.066845, 0, 0, 0, 0, 0]^T$	π	e
5	$[0.0066845, 0, 0.0066845, 0, 0, 0]^T/\sqrt{2}$	$[0.066845, 0, 0.066845, 0, 0, 0]^T/\sqrt{2}$	0	e
7	$[0.0066845, -0.5, 0, 0, 0, 0]^T$	$[0.066845, 0, 0, 0, 0, 0]^T$	0	e
8	$[0.0066845, -0.5, 0.0066845, -0.5, 0.0066845, -0.5]^T/\sqrt{3}$	$[0.066845, 0, 0.066845, 0, 0.066845, 0]^T/\sqrt{3}$	0	f

a few solutions having different quantitative features can coexist. Thus, the GA optimization can result either in different families of orbits, different orbits belonging to the same family, or both. The term "type" is used to categorize the orbit according to the following metrics: planarity or spatiality and the direction of the initial transverse velocity at a given initial position along the sun–Earth line. A planar orbit with $x_0 > 0$ and $y_0' < 0$ is called a distant retrograde orbit (DRO), in consistency with the literature[23]; a spatial orbit having the same characteristics is called a three-dimensional DRO; a planar orbit with $x_0 > 0$ and $y_0' > 0$ will be called a distant prograde orbit (DPO)[23]; and a spatial orbit having the same characteristics is referred to as a three-dimensional DPO.

The mechanism of GA convergence to a population of optimal solutions is monitored using two methods. First, individuals that constitute the final generation can be compared to their predecessors, the individuals of the first generation. Second, the time history of the statistical properties of the fitness can be examined. Figures 2 and 3, respectively, illustrate these measures of convergence for optimization set no. 8.

Figure 2 discloses interesting trends regarding the nature of the optimal parameters. In each plot, the abscissa is the number of individuals in a generation, and the ordinate is the values assumed by each individual. We probe the diversity of the population by plotting the values of each individual for every optimization parameter (initial conditions). Apparently, the algorithm detects a few solutions. There are three dominant solutions for x, 2 dominant solutions for y and y', and a single dominant solution for z, x', and z'. These solutions represent various orbits belonging to the same family. As expected, in this case the niching GA has found a few optimal and suboptimal solutions. This feature is unique to the niching GA algorithm, illustrating its superiority to conventional local optimization methods.

Figure 3 shows the probabilistic nature of the algorithm. The mean of the fitness (defined as the averaged value of the fitness

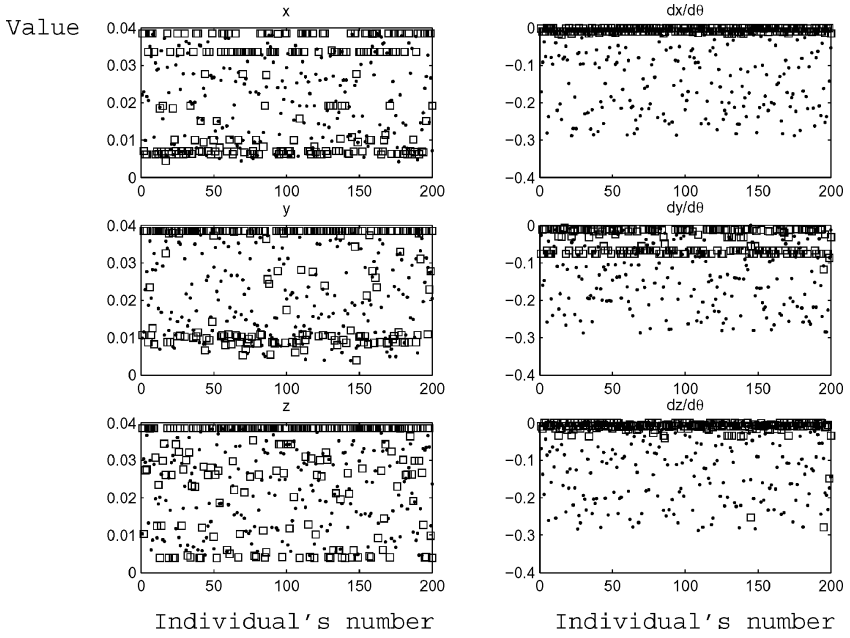

Fig. 2 Comparison of populations of the first (points) the last (squares) generations, optimization set no. 8. The abscissa is the individual (string) number.

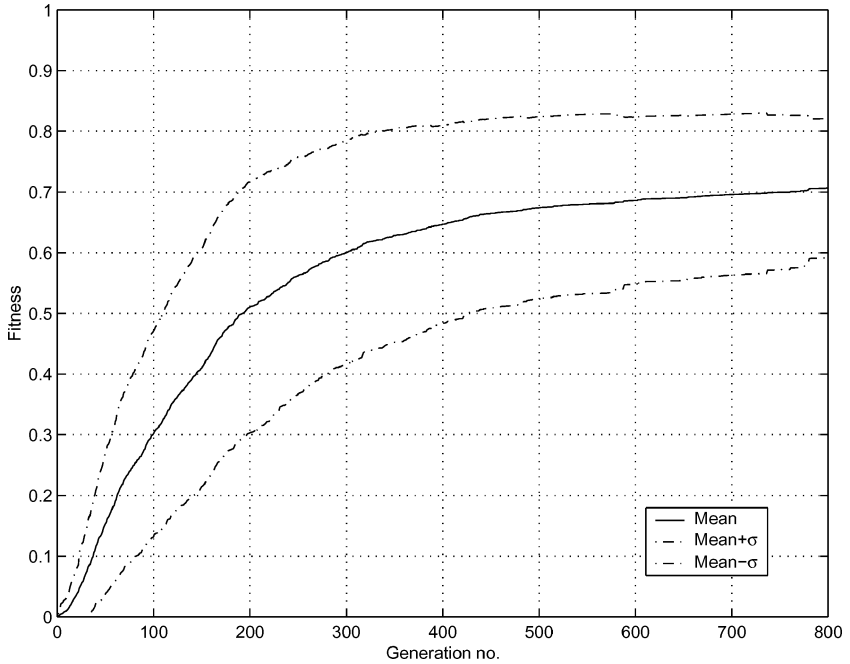

Fig. 3 Time history of the statistical properties of the fitness function for optimization set no. 1 shows the convergence of the GA optimization.

of all individuals in a population) increases with the generations, though local decrease in fitness is possible. Convergence implies that the search converges onto families of solutions. The standard deviation of the fitness (defined as the standard deviation of the fitness of all individual in a population), denoted by σ, is a measure for diversity of solutions. Because the standard deviation remains large, it implies that several solutions coexist.

To visualize the trajectories obtained, the individual with the highest fitness in the last generation is selected as the representative solution. It is possible that several individuals have the same fitness; in which case, one is selected arbitrarily.

The various families of orbits are depicted in Figs. 4–7. In each figure, the top panel describes results for a one-year optimization, and the bottom panel presents extension of the orbits to five years. Optimal initial conditions of representative orbits in each family are given in Table 3. Note that the double-precision values given in Table 3 can be used to regenerate the results presented in this study. We use the Strömgren–Hénon notation[15] to characterize the families of orbits obtained.

Quantitative features of representative orbits of the different families, namely, minimum and maximum distance $r_{\min}$, $r_{\max}$ from Earth, initial distance form Earth r_0, initial velocity v_0, minimum and maximum distance from the sun $\rho_{\min}$, $\rho_{\max}$ and orbit type, are summarized in Table 4. Note that in this table we changed the unit conventions, so that distances from Earth are given in kilometers and the distance from the sun is given in AUs.

The top panel in Fig. 4a depicts three orbits belonging to the Strömgren–Hénon stable family f. These are classical quasi-periodic quasi-elliptic simple DROs, with approximately two crossings of the xz plane per year (1:1 commensurability). All three orbits described in the top panel satisfy

$$\dot{y}_0 = -1.9967x_0 \approx -2x_0 \tag{26}$$

The condition $\dot{y}_0 = 2x_0$ for the existence of simple quasi-periodic DROs was discovered by Hénon[15] in Hill's CR3BP. The bottom panel of Fig. 4a depicts an extension of the middle orbit (top panel) to five years. The five-year orbit consists of an ellipse librating in the cross-track direction. The quantitative features of this orbit are given in the first row of Table 4.

Figure 4b describes a member of family f with a smaller period, having four xz plane crossings per year. Figure 4c depicts yet another member of family f. This is a quasi-circular orbit with eight crossings of the xz plane per year. This orbit is particularly useful, as it remains within almost a constant distance of 1 million km from Earth for a five-year mission lifetime. The increasing number of the Earth–sun line crossings results from decreasing the radius of the orbit. It is also known[15] that the DROs tend to be more circular as they are reduced in size, fitting the observations already made.

Table 3 Optimal initial conditions of orbits representing each family of solutions

Family	Orbit	$(\boldsymbol{x}_0^*)^T$
f	a	[0.03894355345084 0 0 −0.07775997558556 0 0]
f	b	[0.01482889291716 0 0 −0.03537804226749 0 0]
f	c	[0.00680199460712 0 0 −0.02902265964752 0 0]
g'	a	[0.00669917980717 0 0 0.01073472190433 0 0]
g'	b	[0.00669917980717 0 0 0.01073472190433 0 0]
e	a	[0.00668449197861 0 0 −0.02343022812238 0 0]
e	b	[0.00472664960686 0 0.00472664960686 0 0 0]
e	c	[0.00501336953102 −0.00097613025014 0 0 0 0]
f	a	[0.03348096835548 −0.00046191606162 0.00774766945226 −0.06652559750991 0.03675673393090 −0.00902011692574]
f	b	[0.00583817607709 0.00021213377191 0.00005468845617 −0.02914895441397 −0.00090918109209 0.00123524681998]

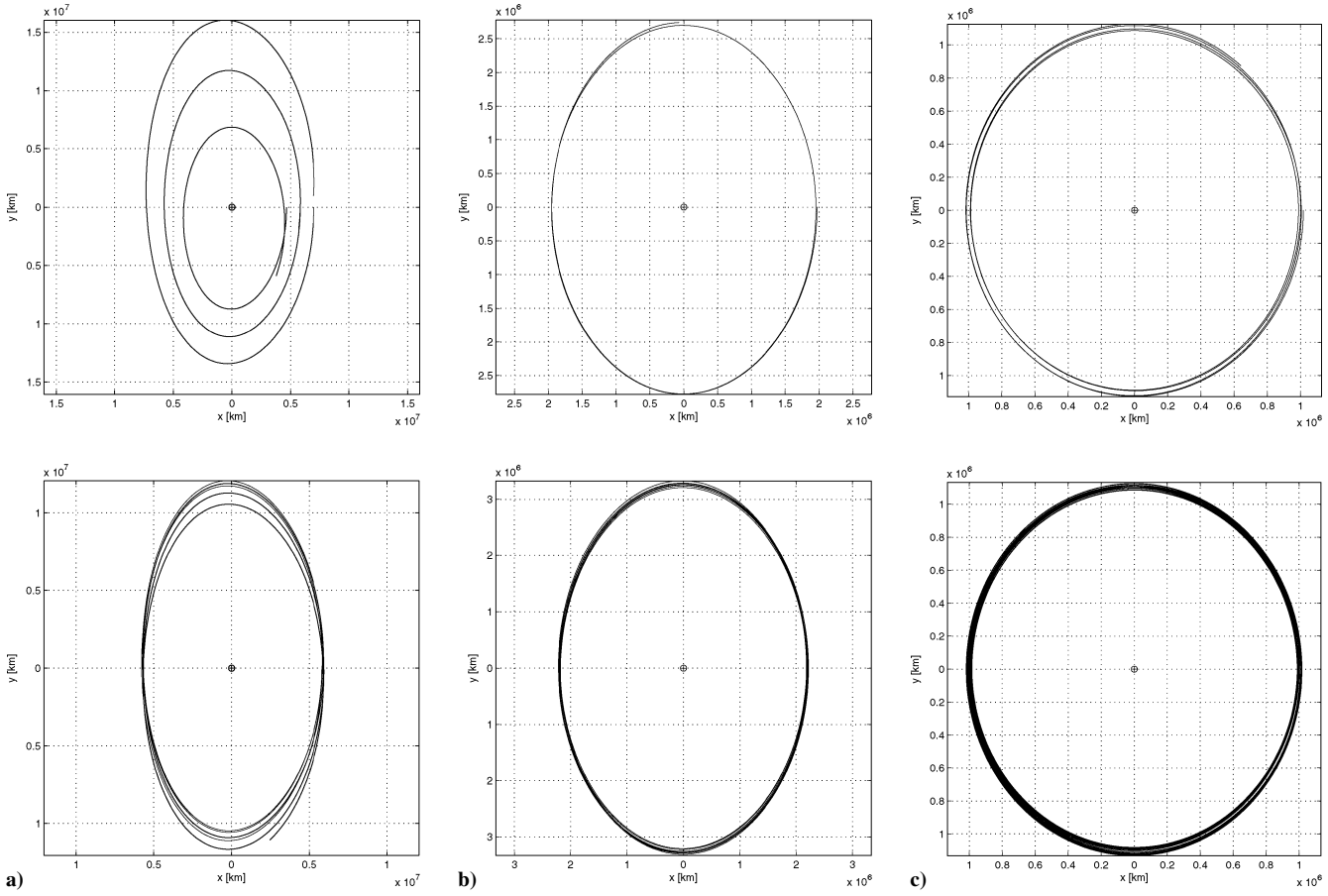

Fig. 4 Family f of distant retrograde orbits: a) 1:1 commensurability orbits; b) orbits with multiple xz crossings; and c) quasi-circular orbit, where top panels: one-year integration; and bottom panels: five-year integration.

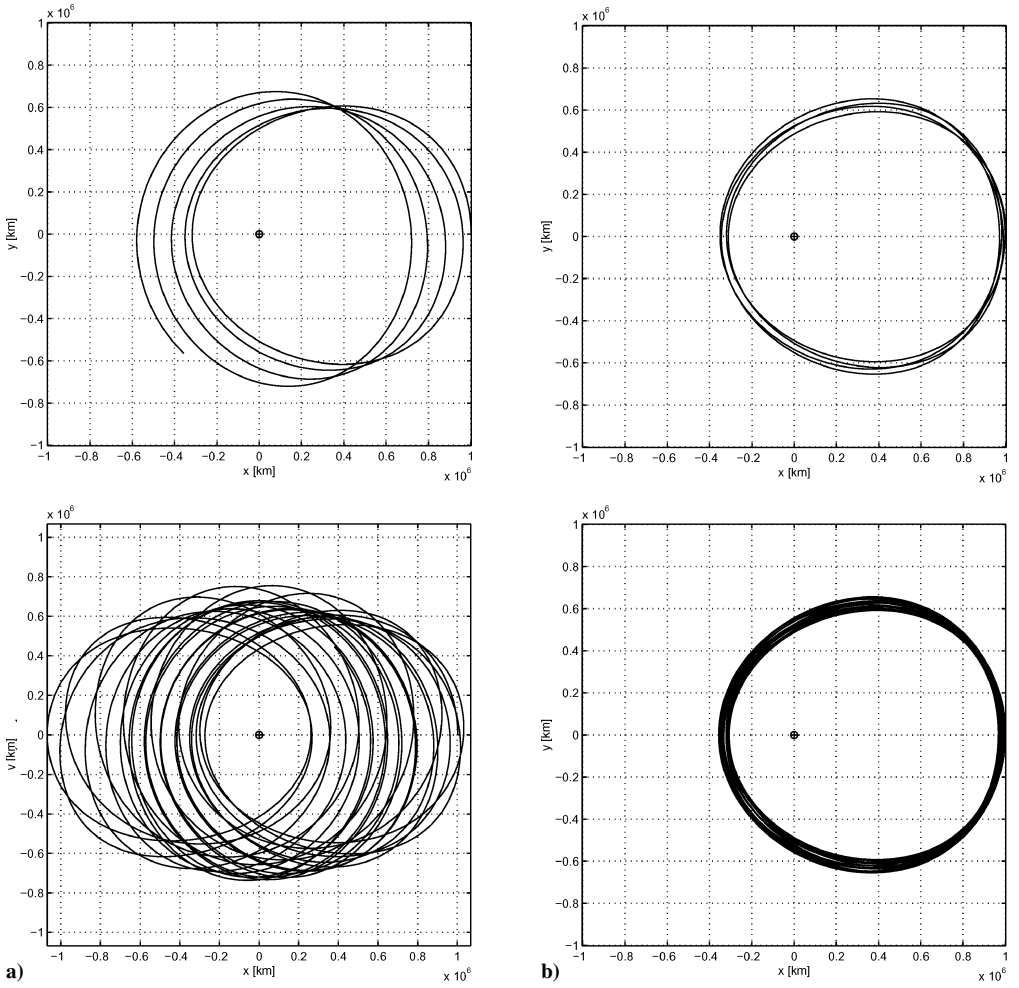

Fig. 5 Family g' of distant prograde orbits: a) osculating orbit and b) stable orbits, where top panels: one-year integration; and bottom panels: five-year integration.

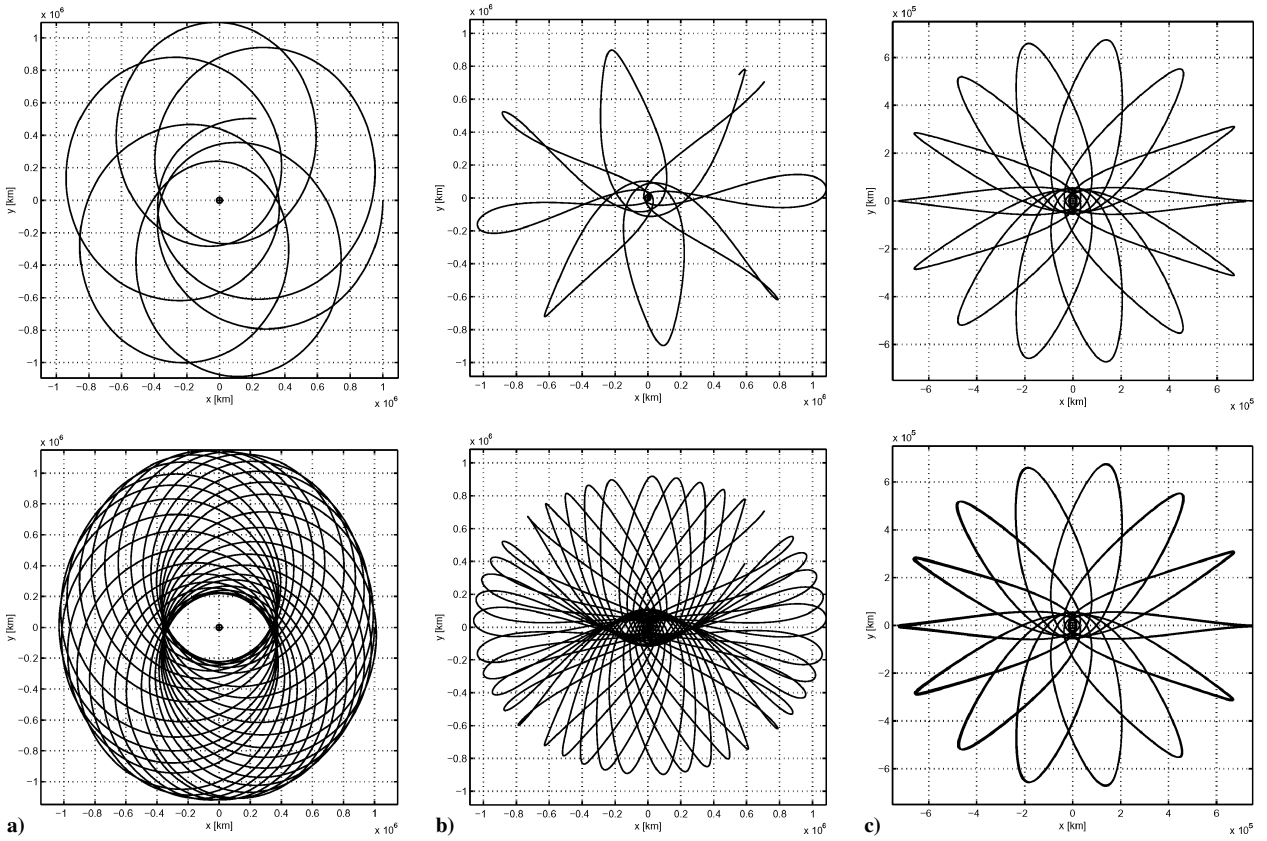

Fig. 6 Family e of highly elliptic orbits: top panels: one-year integration; and bottom panels: five-year integration.

Table 4 Quantitative features of orbits representing each family of optimal solutions

Family	Orbit	$r_{\min}$, km	$r_{\max}$, km	r_0, km	v_0, km/s	$\rho_{\min}$, AU	$\rho_{\max}$, AU	Type
f	a	5,769,577	11,740,892	5,825,955	2.3557	0.97794	1.0229	DRO
f	b	2,191,130	3,270,091	2,218,402	1.0718	0.96888	1.0268	DRO
f	c	986,996	1,126,563	1,017,578	0.8792	0.97898	1.0232	DRO
g'	a	317,151	1,002,197	1,002,197	0.3252	0.97963	1.022	DPO
g'	b	311,893	1,002,197	1,002,197	0.3145	0.98384	1.0234	DPO
e	a	224,900	1,138,236	1,000,000	0.6865	0.97707	1.0234	DRO
e	b	11,532	1,084,448	1,000,000	0	0.98388	1.0163	DPO
e	c	15,883	750,000	750,000	0	0.98346	1.0165	DRO
f	a	6,892,060	8,510,975	7,527,807	2.0339	0.98732	1.0187	3D[a] DRO
f	b	854,531	939,889	883,956	0.8838	0.97779	1.021	3D DRO

[a]3D = three-dimensional.

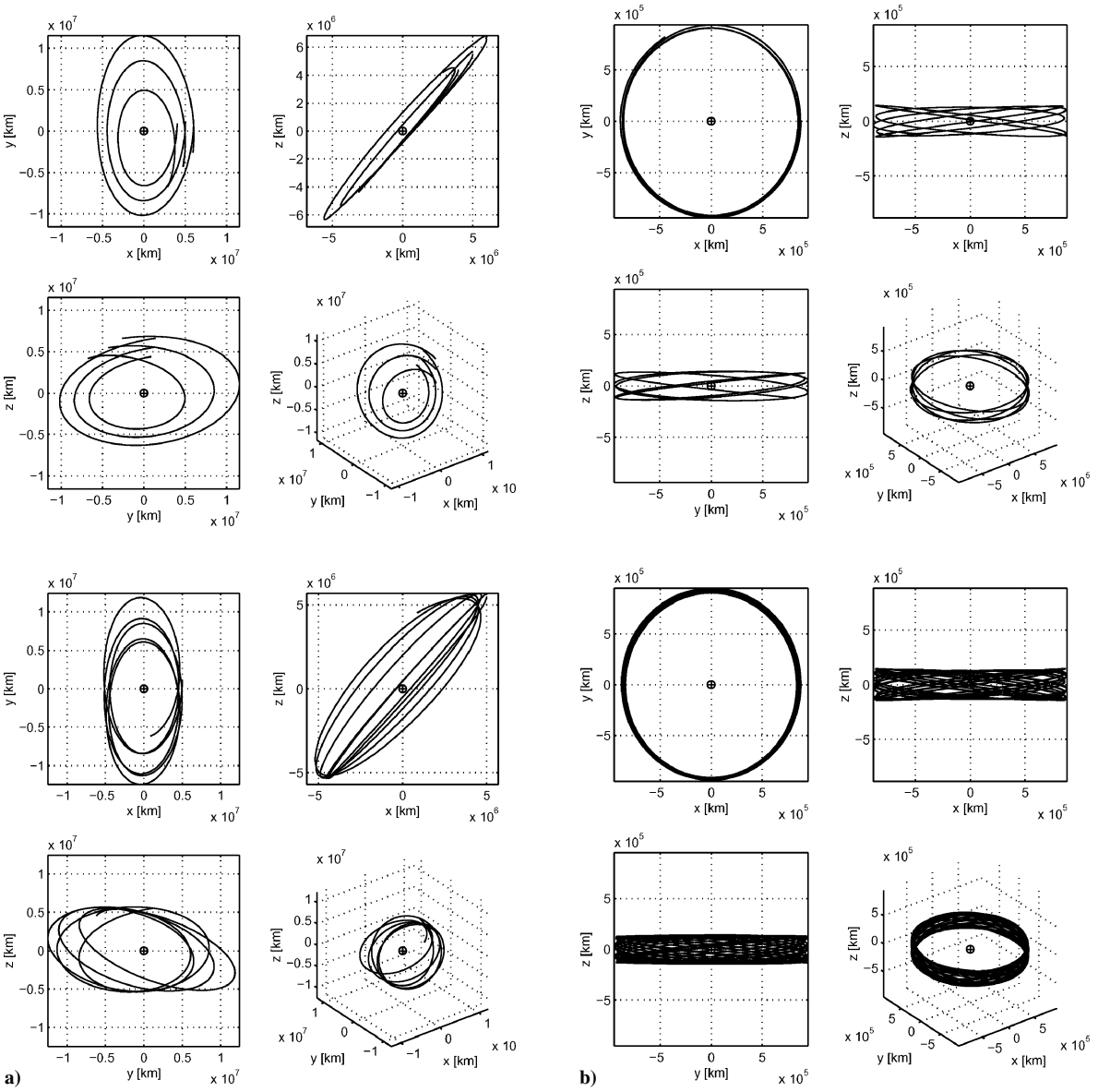

Fig. 7 Family f of three-dimensional distant retrograde orbits: top panels: one-year integration; and bottom panels: five-year integration.

Figure 5a depicts an orbit in the Strömgren–Hénon family g', consisting of DPOs. The representing orbit is characterized by 10 xz plane crossings per year. The motion can be interpreted as a librating ellipse about the Earth in the along-track sense. Figure 5b shows a DPO in family g' having eight xz plane crossing per year. Practically speaking, this orbit is particularly useful because of its relatively close Earth approach (see Table 4 for details). Regarding the topology of these DPOs, it is known[15] that there is a critical radius in which the quasi-circular orbits of family f bifurcate into an unstable family of orbits. Increasing the radius further generates another family of stable orbits. Figure 5a can represent a transition between stable and unstable manifolds associated with the bifurcated quasi-circular orbit. Figure 5b shows an orbit within the stable family of orbits with radius larger than the bifurcation radius.

Figure 6 shows a family e of orbits, which are fundamentally different from the previous families. It comprises highly elliptic DROs about the Earth, with a line of apsides that rotates clockwise when referenced to the rotating-pulsating frame. These orbits are

Hill stable, that is, they are bounded by the oscillating zero-velocity curve surrounding the Earth. Nevertheless, these are three-body orbits, which are perturbed by Earth and the sun. Figure 6a shows an orbit with 12 crossings of the xz plane per year. Figure 6b shows an orbit, which starts with zero initial velocity, which imposes a very close Earth flyby that periodically increases the inertial velocity of the spacecraft. The orbit crosses the xz plane 16 times per year. Figure 6c depicts an orbit with a periodic Earth approach every 25 days. This orbit is characterized by 16 xz plane crossings.

The close Earth approaches of family e (e.g., 11,532 for orbit b, compare Table 4) implies that during a considerable time of the mission lifetime the spacecraft would be affected by Earth's thermal environment, magnetic and radiation fields, drag and oblateness, which can degrade the scientific return by imposing a harsh operational environment. Hence, these orbits are unacceptable as mission orbits, but can be useful as transfer trajectories.

The top panel in Fig. 7a depicts three three-dimensional DROs belonging to family f. These are classical three-dimensional quasi-periodic DROs, with two crossings of the xz plane, two crossings of the xy plane, and two crossings of the yz plane per year. All three orbits described in the top panel satisfy, similarly to the planar case (26), $\dot{y}_0 = -1.987x_0 \approx -2x_0$.

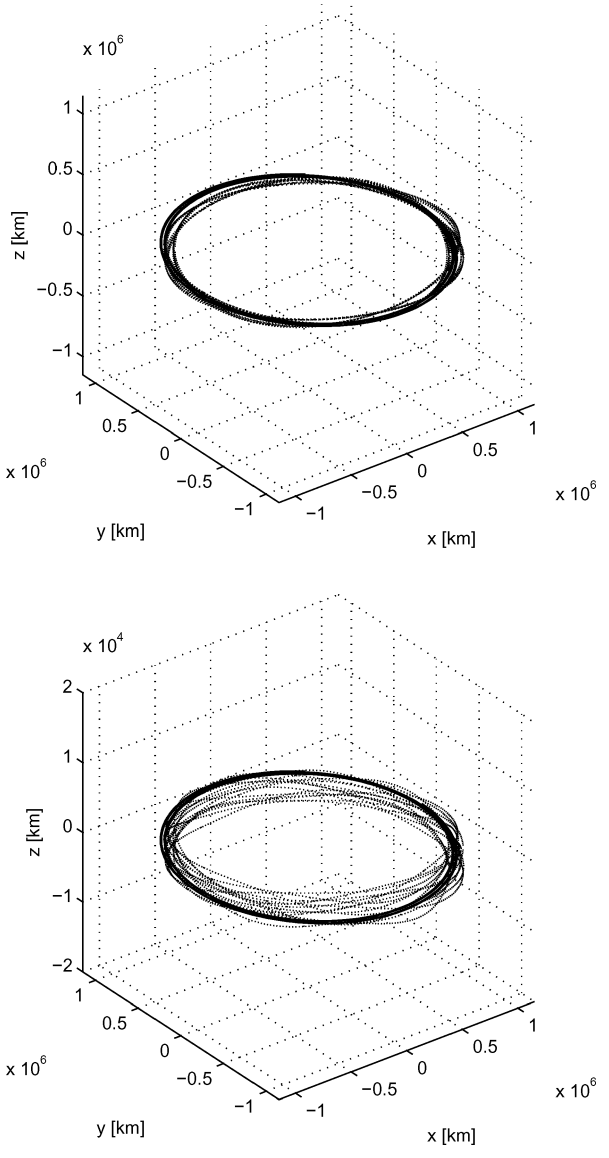

Fig. 8 Quasi-circular DRO of family f, found in the elliptic restricted three-body problem (——), also exists in a full-ephemerides simulation (· · · · curve). Bottom graph rescaled to show the small normal deflection in the full-ephemerides simulation.

The bottom panel of Fig. 7a depicts an extension of the middle orbit (top panel) to five years. The maximum out-of-ecliptic deflection of this orbit is about 0.04 AU, which can be used to reduce to the noise sensitivity of the space-borne observatory as a result of the interference of the interplanetary zodiacal cloud.[29]

Figure 7b depicts another three-dimensional DRO orbit of family f. The characteristic orbit exhibits a quasi-circular projection in the xy plane and a small out-of-ecliptic deflection (maximum 0.0009662 AU, about 145,000 km). Within one year, there are eight xz plane crossings, eight xy plane crossings, and eight yz plane crossings. Examination of Table 4 shows that this orbit is characterized by less than 10% difference between the maximum and minimum distances from Earth during a one-year mission, a very useful feature in terms of real-life missions.

B. Simulation of the Orbits in a Full-Ephemerides Simulation

The ER3BP has yielded numerous useful orbits for deep-space science missions. It is, however, of great value for real-life missions to validate the existence of the newly found orbits in a full-ephemerides simulation. To this end, we have used the JPL-FAST full-ephemerides simulation. This code includes complete, high-order models of the gravitational fields of the Earth, sun, moon, and the planets. (We have not simulated solar radiation pressure.) The inertial system is based on the vernal equinox of date (year 2000), and the time is monitored in Julian days.

The initial conditions of the planar quasi-circular family f DRO, depicted in Fig. 7c, were used to initialize the FAST simulation. The simulation was carried out for a time interval of five years. The results of the full-ephemerides simulation were compared to the results of the ER3BP model. The results of this comparison are depicted in Fig. 8. The upper plot shows the ER3BP orbit (solid line) and the FAST orbit (dotted line) using scaled axes. In the bottom plot, the z axis was enlarged to show the small out-of-ecliptic deflection of the FAST orbit. This comparison shows that the DRO found by the GA search mechanism using the ER3BP model also exists in a full-ephemerides simulation. Both orbits match to a very close degree. The small normal deflection ($\sim$4000 km) obtained in the full ephemerides is because of an inclination pump-up effect, which results mainly from the moon's inclination relative to the ecliptic plane.

V. Conclusions

This paper presents an application of an evolutionary search mechanism, niching genetic algorithms, to the characterization of orbits useful for deep-space science missions. We conclude that the GA-based search constitutes a useful tool for characterizing families of solutions to the elliptic restricted three-body problem. The optimization procedure has yielded interesting and useful orbits for science missions. We used modest population and generation sizes, hence enabling a faster convergence of the optimization. We conclude that even for a relatively small number of iterations the GA-based search algorithm provided a thorough probe of the complex state space of the elliptic restricted three-body problem (ER3BP).

GA optimization yielded three-dimensional families of orbits that were not previously reported in the literature. This implies that the global search for initial conditions constitutes an important generalization of existing, gradient-based techniques for finding orbits in multibody astrodynamical problems.

Perhaps the most significant conclusion from this work is that a most useful family of DROs also exists in a full-ephemerides model (family f). We were able to reconstruct the quasi-circular, planar DRO in a full-ephemerides simulation (JPL-FAST) using the initial conditions obtained by the GA search routine for the ER3BP. Both simulated orbits exhibited similar quantitative and qualitative features, with the FAST orbit developing a small out-of-ecliptic deflection caused by the lunar orbit inclination relative to the ecliptic. Consequently, this paper established a rigorous and new approach to analyzing multibody problems.

Acknowledgments

The contribution of the first author was partially supported by the Center for Absorption in Science, State of Israel. The contribution of

the second author was supported by the Jet Propulsion Laboratory, California Institute of Technology, NASA. The authors thank Ed Belbruno for his help with the FAST code.

References

[1]The TPF Science Working Group, *Terrestrial Planet Finder*, NASA/JPL Publication 99-3, May 1999.

[2]Szebehely, V., *Theory of Orbits*, Academic Press, New York, 1967, Chap. 4, pp. 230–268.

[3]Howell, K. C., Barden, B. T., and Lo, M. W., "Application of Dynamical Systems Theory to Trajectory Design for a Libration Point Mission," *The Journal of the Astronautical Sciences*, Vol. 45, No. 2, 1997, pp. 161–178.

[4]Gómez, G., Masdemont, J., and Simó, C., "Lissajous Orbits Around Halo Orbits," *Advances in the Astronautical Sciences*, Vol. 95, 1997, pp. 117–134.

[5]Shelus, P. J., and Kumar, S. S., "Some Periodic Orbits in the Elliptic Restricted Problem of Three Bodies," *The Astronomical Journal*, Vol. 75, No. 4, 1970, pp. 315–318.

[6]Benest, D., "Elliptic Restricted Problem for Sun-Jupiter: Exsitence of Stable Retrograde Satellites at Large Distances," *Astronomy and Astrophysics*, Vol. 13, 1971, pp. 157–160.

[7]Cors, J. M., Pinyol, C., and Soler, J., "Periodic Solutions in the Spatial Elliptic Restricted Three-Body Problem," *Physica D*, Vol. 154, 2001, pp. 195–206.

[8]Gómez, G., and Olle, M., "Second-Species Solutions in the Circular and Elliptic Restricted Three-Body Problem. II. Numerical Explorations," *Celestial Mechanics and Dynamical Astronomy*, Vol. 52, No. 2, 1991, pp. 147–166.

[9]Olle, M., and Pacha, J. R., "The 3D Elliptic Restricted Three-Body Problem: Periodic Orbits Which Bifurcate from Limiting Restricted Problems," *Astronomy and Astrophysics*, Vol. 351, 1999, pp. 1149–1164.

[10]Kallrath, J., "Bounded Orbits in the Elliptic Restricted Three-Body Problem," *Celestial Mechanics*, Vol. 43, No. 1–4, 1988, pp. 399–408.

[11]Contopoulos, G., "Integrals of Motion in the Elliptic Restricted Three-Body Problem," *The Astronomical Journal*, Vol. 72, No. 5, 1967, pp. 669–673.

[12]Vrcelj, Z., and Kiewiet, J. H., "An Invariant Relation in the Elliptic Restricted Problem of Three Bodies," *The Astronomical Journal*, Vol. 83, No. 5, 1978, pp. 514–521.

[13]Ries, J. G., "Numerical Investigation of Depletion in the Outer Asteroid Belt," *Icarus*, Vol. 121, 1996, pp. 202–206.

[14]Howell, K. C., and Hiday-Johnston, L. A., "Time-Free Transfers Between Libration-Point Orbits in the Elliptic Restricted Problem," *Acta Astronautica*, Vol. 32, No. 4, 1994, pp. 245–254.

[15]Hénon, M., "Numerical Exploration of the Restricted Problem. V. Hill's Case: Periodic Orbits and Their Stability," *Astronomy and Astrophysics*, Vol. 1, 1969, pp. 223–238.

[16]Goldberg, D. E., *Genetic Algorithms in Search, Optimization and Machine Learning*, Addison Wesley Longman, Reading, MA, 1989, pp. 106–132.

[17]KrishnaKumar, K., "Multiple Optimal Solutions for Structural Control Using Genetic Algorithms with Niching," *Journal of Guidance, Control and Dynamics*, Vol. 17, No. 6, 1994, pp. 1374–1377.

[18]Vasile, M., "A Systematic-Heuristic Approach for Space Trajectory Design," *Astrodynamics, Space Missions and Chaos*, edited by E. Belbruno and P. Gurfil, Vol. 1017, New York Academy of Sciences, New York, 2004, pp. 234–254.

[19]Hartman, J. W., Coverstone-Carroll, V. L., and Williams, S. N., "Optimal Interplanetary Spacecraft Trajectories via a Pareto Genetic Algorithm," *The Journal of the Astronautical Sciences*, Vol. 46, No. 3, 1998, pp. 267–282.

[20]Gurfil, P., and Kasdin, N. J., "Optimal Out-of-Ecliptic Trajectories for Space-Borne Observatories," *The Journal of the Astronautical Sciences*, Vol. 49, No. 4, 2001, pp. 509–537.

[21]Mahfoud, S. W., "Niching Methods for Genetic Algorithms," Illinois Genetic Algorithms Lab., Univ. of Illinois, Rept. 95001, Urbana, 1995; URL: http://citeseer.ist.psu.edu/mahfoud95niching.html.

[22]Spears, W. M., and DeJong, K., "An Analysis of Multi-Point Crossover," *Foundations of Genetic Algorithms*, edited by B. Spatz, Margan Kaufmann, San Mateo, CA, 1991, pp. 301–315.

[23]Ocampo, C. A., and Rosborough, G. W., "Transfer Trajectories for Distant Retrograde Orbits of the Earth," *Advances in the Astronautical Sciences*, Vol. 82, No. 2, 1993, pp. 1177–1200.